

# Kramers doublet and magnetic properties of the double perovskite Ba<sub>2</sub>NaOsO<sub>6</sub>

S. W. Lovesey

*ISIS Facility, STFC, Didcot, Oxfordshire OX11 0QX, UK*

*Diamond Light Source, Harwell Science and Innovation Campus, Didcot, Oxfordshire OX11 0DE, UK*

*Department of Physics, Oxford University, Oxford OX1 3PU, UK*

**Abstract** Bulk magnetic properties of Ba<sub>2</sub>NaOsO<sub>6</sub> are examined in the context of an appropriate space group and an atomic model of the Kramers doublet for the osmium ion. It possesses symmetry demanded by the Wykoff position assigned to the osmium ion in a canted ferromagnet. Calculated and measured values of the saturation magnetic moment, and x-ray magnetic dichroic signals (XMCD) at osmium L<sub>2</sub> and L<sub>3</sub> absorption edges agree well.

## I. INTRODUCTION

Magnetic properties of a compound can be strongly influenced by the spin-orbit coupling. Its strength increases with atomic number, and it cannot be overlooked in creating a realistic Kramers doublet of an osmium ion Os<sup>7+</sup>, 5d<sup>1</sup>. We calculate bulk magnetic properties of Ba<sub>2</sub>NaOsO<sub>6</sub> that forms an orthorhombic magnetic structure depicted in Fig. 1 below a transition temperature  $\approx 7$  K. Ferromagnetic layers are strongly canted with respect to the neighbouring layers.

Structural, chemical and magnetic properties of Ba<sub>2</sub>NaOsO<sub>6</sub> along with Ba<sub>2</sub>MgReO<sub>6</sub> (Re<sup>6+</sup>) have been studied using various experimental techniques and theoretic methods [1-11]. The chemical structure of the insulator Ba<sub>2</sub>NaOsO<sub>6</sub> at room temperature is Fm $\bar{3}$ m [2]. Da Cruz Pinha Barbosa *et al.* derive the cited long-range magnetic structure from neutron powder diffraction patterns (Fig. 1(d) [9]), and Lu *et al.* exploit NMR to the same end (Fig. 4(d) [7]). Synchrotron x-ray diffraction patterns reveal the chemical and magnetic structures of single crystals of Ba<sub>2</sub>MgReO<sub>6</sub> (Fig. 1 (c) [8]). The osmium saturation magnetic moment is small [2], and it would be identically zero if the Kramers doublet was an unspoiled quartet (Eq. (8) [3]). In this case, the ground state is a quartet (total angular momentum  $J = 3/2$ ) with an excited doublet ( $J = 1/2$ ).

An atomic model of a Kramers doublet can be useful in reaching a tenable understanding of magnetic properties when covalent bonding is strong [6, 11]. In the present case of a double perovskite, parameters therein account for Os 5d strongly hybridized with p orbitals that are close in energy [2].

We show that an Os ground state inferred from symmetry accounts for the saturation magnetic moment. It uses both  $J = 1/2$  and  $J = 3/2$  atomic states. Furthermore, calculated x-ray magnetic dichroic signals (XMCD) at osmium L<sub>2</sub> and L<sub>3</sub> absorption edges resolve findings from experiments [11].

## II. MATERIAL PROPERTIES

Using available measurements, it is beyond reasonable doubt that the ordered magnetic structures of  $\text{Ba}_2\text{NaOsO}_6$  and  $\text{Ba}_2\text{MgReO}_6$  are the same. Symmetry properties of the rhenate material have been thoroughly discussed with a view to future Bragg diffraction experiments [12]. We assert that, osmium ions occupy centrosymmetric sites in orthorhombic  $\text{Pnn}'m'$  (No. 58.398, magnetic crystal class  $mm'm'$  [13]), namely, Wyckoff positions 2a. A product of a dyad axis of rotation symmetry along the crystal  $c$  axis and time reversal symmetries  $2'/m'$  ( $C_i$ ) restricts dipoles to the basal plane. According to  $^{23}\text{Na}$  NMR spectra measured and analysed by Lu *et al.* there are two distinct magnetic sites Na(Os) [7]. The authors appeal to the canted magnetic structure in Fig. 1 for an interpretation of the spectra. This is not a viable interpretation, however, because  $\text{Pnn}'m'$  possesses only one Na(Os) site.

## III. MULTIPOLES

Neumann's Principle places restrictions on Os multipoles  $\langle T^K_Q \rangle$  of rank  $K$  and  $(2K + 1)$  projections in the interval  $-K \leq Q \leq K$  used to formulate bulk properties, e.g., dichroic signals, and Bragg diffraction patterns [12, 14-16]. Angular brackets about the spherical tensor operator denote a time-average (expectation value). Site symmetry  $2'/m'$  for Wyckoff positions 2a includes inversion, and invariance of axial multipoles  $\langle T^K_Q \rangle$  under the dyad operation  $2'_z$ . It is achieved by the identity  $\sigma_\theta (-1)^Q = +1$ , where the time signature  $\sigma_\theta = +1$  (time-even, charge like) or  $\sigma_\theta = -1$  (time-odd, magnetic). For  $\sigma_\theta = -1$  projections  $Q$  are odd, and magnetic dipoles ( $K = 1$ ) are confined to the basal plane. Our phase convention for real and imaginary parts labelled by single and double primes is  $\langle T^K_Q \rangle = [\langle T^K_Q \rangle' + i\langle T^K_Q \rangle'']$ . A tetragonal cell ( $\xi, \eta, \zeta$ ) used in [12] is shown in Fig. 1, with Cartesian dipoles  $\langle T^1_\xi \rangle = -\sqrt{2} \langle T^1_{+1} \rangle'$  and  $\langle T^1_\eta \rangle = -\sqrt{2} \langle T^1_{+1} \rangle''$ .

XMCD signals, and Bragg diffraction patterns, are derived from an electronic structure factor  $\Psi^K_Q$  [12, 16]. Calculated for Os ions at sites with positions  $\mathbf{d}$  in a unit cell (Bragg wavevector = 0 for bulk properties),

$$\Psi^K_Q(\text{Pnn}'m') = \sum_{\mathbf{d}} \langle T \rangle_{\mathbf{d}} = [\langle T^K_Q \rangle + \sigma_\theta (-1)^{K+Q} \langle T^K_{-Q} \rangle]. \quad (1)$$

A complex conjugate  $\langle T^K_Q \rangle^* = (-1)^Q \langle T^K_{-Q} \rangle$ , and  $\Psi^K_Q(\text{Pnn}'m')$  is purely real for  $\sigma_\theta (-1)^K = +1$ . Bulk magnetism is determined by  $\Psi^1_{+1}(\text{Pnn}'m') = 2 \langle T^1_{+1} \rangle' = -\sqrt{2} \langle T^1_\xi \rangle$ .

## IV. MAGNETIC MOMENT AND XMCD

Symmetry of Wyckoff positions 2a in  $\text{Pnn}'m'$  requires  $(-1)^Q = -1$  for a magnetic multipole. In consequence,  $[|u\rangle + f|\hat{u}\rangle]$  is a suitable wavefunction for an osmium ion, where  $|u\rangle$  is a Kramers state,  $|\hat{u}\rangle$  its conjugate, and  $\phi$  in  $f = \exp(i\phi)$  is to be determined [12, 17]. The conjugate (time-reversed) state is constructed with the rule  $c|j, m\rangle \rightarrow c^* \{(-1)^{j-m} |j, -m\rangle\}$ , where  $c$  is a classical number. Using the identity  $\langle u|T^K_Q|u\rangle = -\langle \hat{u}|T^K_Q|\hat{u}\rangle$ , the corresponding expectation value,

$$\langle T^K_Q \rangle = (1/2) [f \langle u | T^K_Q | \hat{u} \rangle + f^* \langle \hat{u} | T^K_Q | u \rangle], \quad (2)$$

with  $f^* = \exp(-i\phi)$ . Matrix elements in Eq. (2) are calculated with a standard prescription and known reduced matrix elements (RMEs) [16, 18]. Atomic states  $|J, M\rangle$  in the Kramers doublet are chosen to be,

$$|u\rangle = [3/2, 1/2] + t [5/2, -3/2] [1 + |t|^2]^{-1/2}, \quad (3)$$

where  $t$  is a complex mixing parameter. Note that  $\langle \hat{u} | T^K_Q | u \rangle$  does not include  $t^*$ , and  $\langle u | T^K_Q | \hat{u} \rangle$  does not include  $t$ . Allowed projections in  $\langle u | T^K_Q | \hat{u} \rangle$  are  $Q = \pm 1, -3$ , with  $Q = \pm 1, +3$  for  $\langle \hat{u} | T^K_Q | u \rangle$ . A compatibility of calculated and measured properties of Os ions is our justification for Eq. (3).

The magnetic moment  $(\mathbf{L} + 2\mathbf{S}) = (\mathbf{J} + \mathbf{S})$ . A matrix element diagonal in  $J$  can be calculated with  $(\mathbf{L} + 2\mathbf{S}) = g\mathbf{J}$  using an RME  $= [J(J+1)(2J+1)]^{1/2}$  and Landé factor  $g = 4/5$  ( $S = 1/2, L = 2$ ). Off-diagonal matrix elements of  $(\mathbf{J} + \mathbf{S})$  are those of  $\mathbf{S}$  and include the mixture of states  $J = 3/2$  and  $5/2$  in Eq. (3) (RME Eq. (7.1.7) [19]). The final result is,

$$\langle (\mathbf{L} + 2\mathbf{S}) \rangle_{+1} = (\sqrt{2}/5) [2f + t f^* \sqrt{3}] [1 + |t|^2]^{-1}. \quad (4)$$

Turning to XMCD signals derived from an electric dipole - electric dipole (E1-E1) absorption event, RMEs for  $T^K$  at  $L_2$  and  $L_3$  edges are derived from Eq. (73) in Ref. [16]. Using Eq. (1) the two signals are,

$$\Psi^1_{+1}(L_2) = - (1/9) f' [1 + |t|^2]^{-1}, \quad (5)$$

$$\Psi^1_{+1}(L_3) = f' [-2 + t 9\sqrt{3}] (225 [1 + |t|^2])^{-1}.$$

Orbital angular momentum  $\langle \mathbf{L} \rangle$  obeys a sum rule [14, 16],

$$\langle T^1(L_2) \rangle + \langle T^1(L_3) \rangle = - \langle \mathbf{L} \rangle / (10\sqrt{2}), \quad (6)$$

which is easily derived from Eq. (73) in Ref. [16].

## V. DISCUSSION AND CONCLUSIONS

XMDC signals Eq. (5) exhibit properties captured in measurements at the L edges of Os with a sample temperature = 3.5 K [11] (Fig. 3 and Section C in SM, with minimal information about powdered  $\text{Ba}_2\text{NaCaOsO}_6$  used as a host material). According to the authors, signals measured at osmium  $L_2$  and  $L_3$  absorption edges have identical signs, and the  $L_3$  signal is close to zero. Evidently,  $\Psi^1_{+1}(L_3) = 0$  for real  $t = (2/9\sqrt{3})$ , which implies that a weak  $L_3$  signal is due to mixing of atomic states  $J = 3/2$  and  $J = 5/2$  in the Kramers state Eq. (3). The sign of  $\Psi^1_{+1}(L_2)$  is fixed by a single parameter. Interestingly, null values of an  $L_2$  signal are known in other materials, including  $\text{Sr}_2\text{IrO}_4$  [17].

A plausible interpretation of the magnetic moment Eq. (4) uses  $t = (2/9\sqrt{3})$  which ensures  $\Psi^1_{+1}(L_3) = 0$  [11]. One can add a constraint  $\langle (\mathbf{L} + 2\mathbf{S}) \rangle_\xi = \langle (\mathbf{L} + 2\mathbf{S}) \rangle_\eta$  that fixes  $f$ , and arrive at  $\langle (\mathbf{L} + 2\mathbf{S}) \rangle_\xi = 0.546$ . To a large extent, the difference between the calculated and

measured values can be attributed to shielding by electron back-transfer between Os and neighbouring O ions (covalency) [2, 6, 11]. Moreover, other interpretations of Eq. (4) might exploit different parameters,  $t$  and  $f$ , to good effect.

In summary, we have assigned the long-range magnetic order of  $\text{Ba}_2\text{NaOsO}_6$  depicted in Fig. 1 to the orthorhombic space group  $\text{Pnn}'m'$  (No. 58.398) [12, 13]. Future measurements of magnetic Bragg diffraction patterns can be confronted with published results for  $\text{Pnn}'m'$  [12]. The mentioned study includes allowed structural distortions. Down to a sample temperature of 10 K there is no evidence of distortions away from cubic symmetry (neutron powder diffraction patterns [9]). Symmetry of the Wyckoff positions imposes restrictions on osmium electronic multipoles, and the magnetic structure leads to Eq. (1) for the XMCD signal. It is an exact result, likewise all our work leading to results in Eqs. (4) and (5) [16, 18]. The brevity of Eq. (3) for the Kramers state is commendable

**Acknowledgements** Correspondence with Dr S. Agrestini, Dr D. D. Khalyavin, and Professor G. van der Laan.

- [1] K. E. Stitzer *et al.*, *Solid. State Sci.* **4**, 311 (2002).
- [2] A. S. Erickson *et al.*, *Phys. Rev. Lett.* **99**, 016404 (2007).
- [3] G. Chen, R. Pereina and L. Balents, *Phys. Rev. B* **82**, 174440 (2010).
- [4] A. J. Steele *et al.*, *Phys. Rev. B* **84**, 144416 (2011).
- [5] H. Ishizuka and L. Balents, *Phys. Rev. B* **90**, 184422 (2014).
- [6] S. Gangopadhyay and W. E. Pickett, *Phys. Rev. B* **91**, 045133 (2015).
- [7] L. Lu *et al.*, *Nat. Commun.* **8**, 14407 (2017).
- [8] D. Hirai *et al.*, *Phys. Rev. Res.* **2**, 022063 (2020).
- [9] V. da Cruz Pinha Barbosa *et al.*, *Chem. Mat.* **34**, 1098 (2022).
- [10] F. I. Frontini *et al.*, *Phys. Rev. Lett.* **133**, 036501 (2024).
- [11] S. Agrestini *et al.* *Phys. Rev. Lett.* **133**, 066501 (2024).
- [12] S. W. Lovesey and D. D. Khalyavin, *Phys. Rev. B* **103**, 235160 (2021).
- [13] We use the Belov-Neronova-Smirnova (BNS) setting of magnetic space groups, see Bilbao Crystallographic server, <http://www.cryst.ehu.es>.
- [14] B. T. Thole, P. Carra, F. Sette, and G. van der Laan., *Phys. Rev. Lett.* **68**, 1943 (1992); P. Carra, B. T. Thole, M. Altarelli, and X. D. Wang, *ibid.* **70**, 694 (1993);

- P. Carra, H. König, B.T. Thole, and M. Altarelli, *Physica* **192B**, 182 (1993).
- [15] J. Luo, G.T. Trammell, and J.P. Hannon, Scattering operator for elastic and inelastic resonant x-ray scattering. *Phys. Rev. Lett.* **71**, 287 (1993).
- [16] S. W. Lovesey, E. Balcar, K. S. Knight, and J. Fernández Rodríguez, *Phys. Reports* **411**, 233 (2005).
- [17] L. C. Chapon and S. W. Lovesey, *J. Phys.: Condens. Matter* **23**, 252201 (2011).
- [18] S. W. Lovesey, *Phys. Scripta* **90**, 108011 (2015).
- [19] A.R. Edmonds, *Angular momentum in quantum mechanics* (Princeton University Press, New Jersey, 1960).

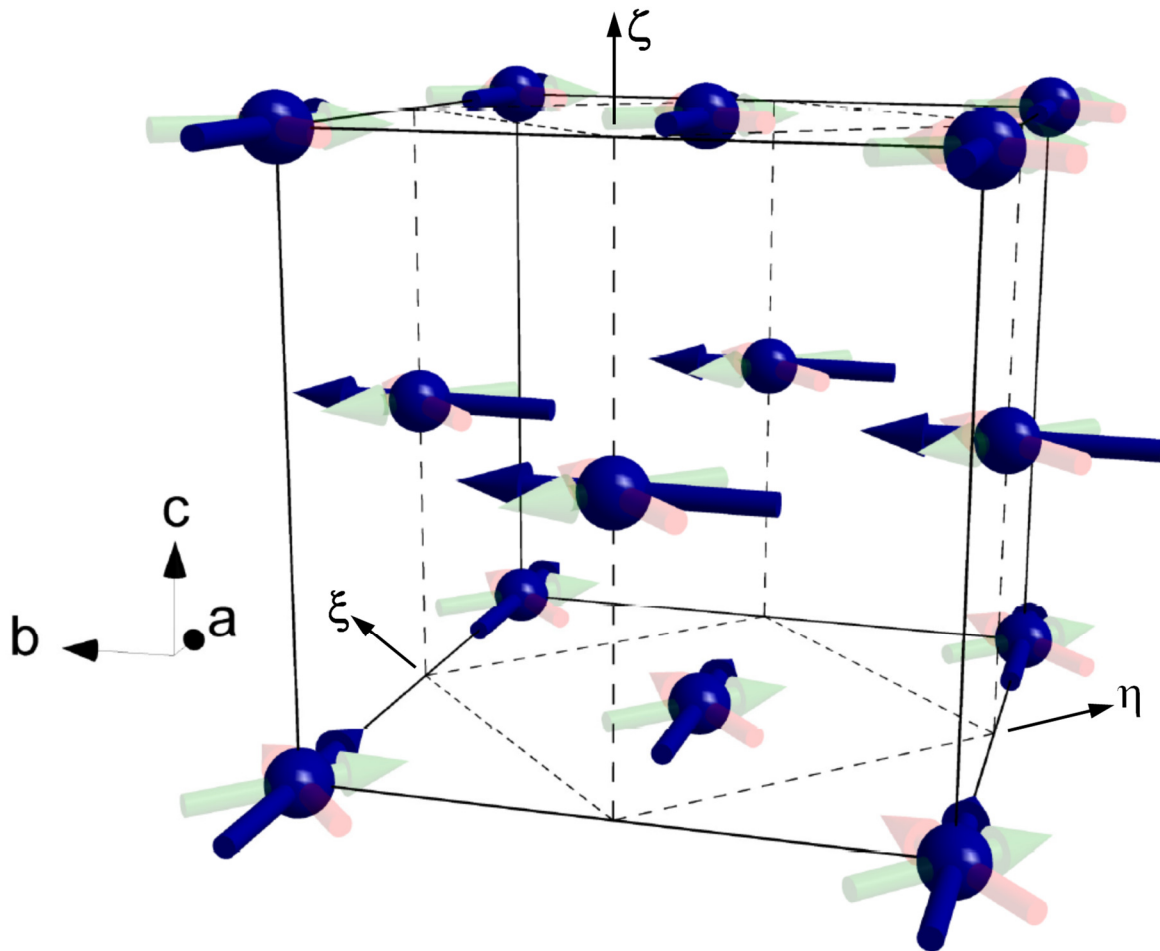


**FIG. 1.** Ferro- and antiferromagnetic osmium dipole components of the ordered magnetic structure  $\text{Ba}_2\text{NaOsO}_6$  are depicted by transparent red and green arrows, respectively. A tetragonal basis labelled  $(\xi, \eta, \zeta)$  is introduced in Section III [12].

